Polymorphism, Structure, Guest Conformation, and Dynamics in the Inclusion Compound of 1,2Dichloroethane with Tris(5-acetyl-3-thienyl) Methane: a Combined Single Crystal and Powder...

ARTICLE *in* THE JOURNAL OF PHYSICAL CHEMISTRY B · AUGUST 2002

Impact Factor: 3.3 · DOI: 10.1021/jp013983a

4 AUTHORS, INCLUDING:

Paul S Sidhu
University of Lethbridge
16 PUBLICATIONS **108** CITATIONS
SEE PROFILE

John A. Ripmeester
National Research Council Canada
713 PUBLICATIONS **15,630** CITATIONS
SEE PROFILE

Polymorphism, Structure, Guest Conformation, and Dynamics in the Inclusion Compound of 1,2-Dichloroethane with Tris(5-acetyl-3-thienyl) Methane: a Combined Single Crystal and Powder X-ray Diffraction, ^{13}C CP/MAS, and ^{2}H NMR Study

Paul S. Sidhu, Gary D. Enright, and John A. Ripmeester*

National Research Council, Steacie Institute for Molecular Sciences, 100 Sussex Drive, Ottawa, Ontario, Canada, K1A 0R6

Glenn H. Penner

Department of Chemistry and Biochemistry, University of Guelph, Guelph, Ontario, Canada, N1G 2W1

Received: October 26, 2001; In Final Form: February 25, 2002

Various physicochemical characterization techniques were used to study the structure and guest dynamics of the 1,2-dichloroethane/tris (5-acetyl-3-thienyl) methane (TATM) inclusion compound. This complex was observed to crystallize in two forms, a triclinic *P*-1 structure and a less usual monoclinic $P2_1/c$ form. The X-ray structures indicate that the TATM molecules form "bottleneck" channels parallel to the crystallographic *c* axis in both forms and that the guests exist exclusively in the trans form. Solid-state deuterium NMR spectroscopy was used to study the dynamics of the 1,2-dichloroethane-d_4 guest in the triclinic form. The simplest model consistent with the experimental NMR spectra was based on internal rotation about the C−C bond (a trans/gauche conformational equilibrium). As this was not consistent with the X-ray structure, another model was developed where the trans conformer performs 180° flips about an axis through the center of symmetry of the guest and perpendicular to the Cl−C−C−Cl plane. The important point to be taken from this work is that complementary methods are often necessary to discriminate between motional models based on a single technique, and that the simplest model is not necessarily correct.

Introduction

The void space in inclusion compounds provides a convenient way of confining guests in order to test our ability to describe their dynamic states. In the case of rigid guests, or guests with a limited number of allowed conformers, considerable progress has been made. However, because of the additional degrees of freedom for aliphatic compounds such descriptions are more complicated. In this contribution we use a variety of methods to study the structure and dynamics of 1,2-dichloroethane included in tris (5-acetyl-3-thienyl) methane (TATM) compounds. In the solid state, this guest molecule is known to undergo dynamic processes that involve 180° jumps of the molecule about the Cl−Cl axis as a rigid unit.[1−4] In the gas phase, however, the guest motion is isotropic and shows conformational isomerism.[5] In at least one inclusion compound, a clathrate hydrate, it is known that size constraints force the 1,2-dichloroethane guest into a gauche conformer.[6] Thus, questions can be asked about the state of the guest in a cavity: is it more like a gas or a solid in the inclusion compound void space? It proved to be a surprisingly challenging task to arrive at a model that was consistent with the data obtained with the various experimental methods employed. First of all we give a brief description of the host system used in our study, and then we give a brief description of the salient features of the techniques used.

* To whom correspondence may be addressed. Phone: (613) 993-2011. Fax: (613) 998-7833. E-mail: jar@ned1.sims.nrc.ca.

TATM, **1**, is a conformationally flexile tripodal host molecule

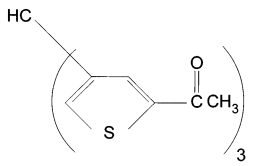

1

structurally analogous to the triphenylmethane group of hosts.[7] It has been found to form inclusion compounds with a large and wide variety of organic compounds.[8] It was first prepared in 1973 by Gol'dfarb and co-workers from chloroform and 2-acetyl thiophene, in the presence of excess aluminum chloride.[9] They also reported that TATM incorporates solvents such as benzene, ethanol, and pyridine on recrystallization. Sublimation of the host−guest complexes under vacuum resulted in an amorphous guest-free pale orange solid, with a broad melting point range of 50−58 °C.

Four years later, Bin Din and Meth-Cohn reported melting points for TATM inclusion compounds with 39 different guests, the majority of which were composed of a 2:1 host:guest molar ratio.[8] Furthermore, their study, to that point in time, failed to reveal a solvent that was not incorporated.

Between 1991 and 1992, four crystal structures of TATM inclusion compounds were determined by H. M. Roos and co-workers. All four crystallized in the triclinic P-1 space group.[10−14] Ethyl acetate and ethanol each form 2:1 host:guest complexes

10.1021/jp013983a CCC: $22.00
Published on Web 07/25/2002

TABLE 1: Crystal Data, Data Collection, and Final Refinement Parameters for the Two Crystal Forms of 1,2-Dichloroethane in TATM

crystal data		
molecular formula	$2C_{19}H_{16}O_3S_3\ 1C_2H_4Cl_2$	$2C_{19}H_{16}O_3S_3\ 1C_2H_4Cl_2$
molecular weight (g/mol)	875.98	875.98
temperature (K)	173	173
crystal system	triclinic	monoclinic
space group	*P*-1	$P2_1/c$
a (Å)	8.0332 (5)	12.6902 (7)
b (Å)	10.9065 (7)	12.7431 (7)
c (Å)	12.3063 (8)	13.7376 (7)
α (deg)	97.207 (10)	90
β (deg)	106.630 (10)	109.046 (10)
γ (deg)	96.686 (10)	90
V (Å^3)	1011.70 (11)	2099.90 (20)
Z	1	2
D_{calcd} (g/cm^3)	1.438	1.379
F(000)	454	900
μ (Mo Kα) (mm^{-1})	0.517	0.497
λ (Å)	0.71073	0.71073
2θ range (deg)	$1.75° < 2\theta < 28.72°$	$1.70° < 2\theta < 28.77°$
data collection		
crystal dimensions (mm)	$0.30 \times 0.35 \times 0.40$	$0.20 \times 0.35 \times 0.40$
index ranges	$-10 \le h \le 10$	$-17 \le h \le 17$
	$-14 \le k \le 14$	$-17 \le k \le 17$
	$-16 \le l \le 16$	$-18 \le l \le 18$
reflections measured	11818	24125
unique reflections	5170	5453
R (int)	0.0350	0.0266
completeness to $2\theta_{max}$	98.8%	95.7%
scan mode	omega	omega
absorption correction	empirical	empirical
final refinement		
refinement method	full-matrix least squares	full-matrix least squares
data/restraints/parameters	5170/3/341	5453/0/284
goodness of fit	0.788	0.983
final *R* indices [$I > 2\sigma(I)$]	$R_1 = 0.0443$; $wR_2 = 0.1190$	$R_1 = 0.0464$; $wR_2 = 0.1131$
R indices (all data)	$R_1 = 0.0523$; $wR_2 = 0.1300$	$R_1 = 0.0677$; $wR_2 = 0.1527$
highest peak (e Å^{-3})	0.583	0.411
deepest hole (e Å^{-3})	−0.461	−0.333

in which the guest interacts with two of the three acetyl thienyl substituents of each of the two host molecules in the unit cell.[11,12] The *n*-hexane clathrate is similar in this sense, but forms a 3:1 host:guest complex.[13] Benzene/TATM appears to be different in that the guest interacts with only one thienyl ring of each host molecule.[14] In all four structures, the isotropic thermal displacement factors of the guests atoms are at least two to three times as large as those measured for the hosts. This suggested the lack of strong bonding between host and guest. Since that time further structural studies have corroborated this view of TATM inclusion compounds.[15−17]

Single crystal X-ray crystallography has contributed greatly to the knowledge of the structural properties of inclusion compounds.[18] With a determination of the atomic positions within the asymmetric unit, it becomes possible to determine the packing motif and to classify the host framework as forming cavities, channels, or layers in which the guest molecules reside. Powder X-ray diffraction provides less information than single-crystal diffraction; however, it can characterize the bulk product (rather than a single selected crystal), and can be used on crystalline solids that cannot be prepared as single crystals of sufficient size and quality for conventional single-crystal X-ray diffraction studies.

The ^{13}C NMR spectra of solids are dominated by a number of electronic and magnetic interactions.[19] Whereas in solution these chemical shifts are immediately apparent at their isotropic averages, in solids, the anisotropic interactions must be averaged by the combination of magic angle spinning and high power dipolar decoupling. One important feature of high-resolution solid-state cross polarization/magic angle spinning (CP/MAS) NMR spectroscopy is that nuclei which are normally considered to be chemically equivalent in solution may not be magnetically equivalent in the solid state, and hence, extra signal splittings may occur. In principle, every crystallographically inequivalent atom can give rise to its own resonance. It is the crystallographic symmetry rather than the molecular symmetry that determines the equivalence or nonequivalence of any group of atoms. Examination of the ^{13}C CP/MAS NMR spectrum can therefore give a quick "snapshot" of the contents of the asymmetric unit and has potential as a "fingerprinting" technique for polycrystalline solids. It can also be considered as a routine screening method before embarking on single-crystal X-ray crystallographic studies.

In contrast to diffusive Brownian reorientation in the liquid state, molecular motion in solids usually proceeds through discrete jumps. These motions are often masked in solution by overall isotropic molecular tumbling. Inclusion compounds can provide anisotropic environments for small molecules that exist as solids only at low temperatures. The analysis of molecular motion is fundamental to the understanding of many macroscopic properties of solids. Knowing whether the nature of the guest's motion is determined by the internal symmetry of the guest molecule or the external symmetry of the host cavity provides insight into the nature of the interaction between host and guest. In this study we use ^{2}H NMR spectroscopy, as described below, to develop detailed dynamic models for the guest molecules. Solid-state deuterium NMR spectroscopy has become a very powerful technique for the study of dynamic processes in a variety of systems.[20−22] These include crystalline solids,[23−25] inclusion compounds,[26−28] and zeolites.[29−31] This

has been made possible with a combination of technical advances such as the development of the quadrupolar echo pulse sequence,[32] the availability of computer programs capable of simulating deuterium NMR powder line shapes,[33] and progress in the chemistry of selective isotope labeling.[34]

Experimental Section

Commercially available reagants were used as received. The 1,2-dichloroethane/TATM inclusion compound was crystallized by two different methods. In the first (slow evaporation), a hot saturated solution of about 300 mg TATM in ~2 mL of 1,2-dichloroethane was poured into a glass Petri dish and the excess 1,2-dichloroethane was allowed to evaporate at room temperature over the course of approximately 1−2 days. This sample was used for single-crystal X-ray diffraction analysis. In the other method (slow cooling), again 300 mg TATM was dissolved in 2 mL of 1,2-dichloroethane and then sealed in a glass ampule. The ampule was then placed in an oven, and cooled from the boiling point of 1,2-dichloroethane (83 °C) to room temperature, at a rate of 5 °C per day. The resulting crystals were then filtered and ground into a fine powder. The preparation of TATM proceeded as described previously.[35]

Single-crystal X-ray diffraction data were measured on a Siemens Smart CCD diffractometer at 173 K, using graphite monochromatized Mo Kα radiation ($\lambda = 0.71073$ Å) in the ω scan mode. The data reduction included correction for Lorentz and polarization effects, with an applied empirical absorption correction. Refined cell dimensions were obtained by least-squares analysis of the setting angles of 7891 reflections in the range $3° < 2\theta < 58°$. The crystal structures were solved by direct methods using the NRCVAX program,[36] and the structure was refined by full-matrix least-squares routines using the SHELXTL program. Direct methods yielded all non-hydrogen host atoms in the unit cell, and all non-hydrogen atoms were refined anisotropically. The host hydrogen atoms were located in the difference Fourier map, while the guest hydrogens were placed in calculated positions with a riding temperature factor and bond length constraints. Crystal data and structural refinement parameters are given in Table 1. Reduced atomic coordinates for the two forms appear in Tables 2 and 3.

X-ray powder diffraction patterns (XRD) were recorded at room temperature on a Rigaku Geigerflex goniometer diffractometer, using graphite monochromatized Co Kα radiation ($\lambda = 1.79$ Å) in the $\theta-\theta$ scan mode. Samples were scanned over a range $10° < 2\theta < 40°$, with a 30 s accumulation time at an increment of 0.02° in 2θ, giving a total acquisition time for each sample of approximately 12 h.

The ^{13}C CP/MAS NMR spectra were recorded at room temperature on a Bruker AMX 300 NMR spectrometer at a frequency of 75.483 MHz for ^{13}C and 300.145 MHz for ^{1}H. The polycrystalline powder samples were spun in a 5 mm Doty magic angle-spinning (MAS) probe at frequencies between 5 and 6 kHz. The numbers of scans collected was approximately 10 000, with 3.8 μs 90° pulses, 5 ms cross polarization contact time, 51.2 ms acquisition time, and a 10 s recycle delay. Typically 4096 data points were accumulated with zero filling to 16 K, resulting in a digital resolution of about 2.4 Hz/point. The chemical shifts are given relative to tetramethylsilane at zero ppm, and were referenced externally (by rotor replacement) to the high field signal of hexamethylbenzene (16.9 ppm).

The ^{2}H NMR spectra were recorded on a Bruker AMX 300 NMR spectrometer at a frequency of 46.07 MHz. The polycrystalline powder samples were packed in 6 mm o.d. NMR tubes of length ~2 cm. The deuterium NMR spectra were obtained using the quadrupole echo pulse sequence:[32] $(\pi/2)_{\pm x}-\tau_Q-(\pi/2)_y-\tau_Q-$acquire. The length of the $\pi/2$ pulses were approximately 3.0 μs, and a recycle delay of 1 s was used. At each temperature, the echo signals were collected using a τ_Q

TABLE 2: Reduced Atomic Coordinates ($\times 10^4$) and Equivalent Isotropic Displacement Parameters (Å^2 $\times$ 10^3) for the Triclinic Form of 1,2-Dichloroethane/TATM at −100 °C[a]

	x	*y*	*z*	*U*(eq)
S(1)	2586(1)	4592(1)	148(1)	27(1)
S(2)	−4156(1)	1675(1)	1505(1)	28(1)
S(3)	4145(1)	2081(1)	4924(1)	34(1)
O(1)	663(1)	4698(1)	−2297(1)	39(1)
O(2)	−6386(1)	−681(1)	1456(1)	37(1)
O(3)	4496(1)	4253(1)	6683(1)	47(1)
C(1)	967(1)	1787(1)	1666(1)	23(1)
C(2)	1274(1)	2753(1)	926(1)	23(1)
C(3)	2611(1)	3754(1)	1238(1)	27(1)
C(4)	755(1)	3600(1)	−766(1)	24(1)
C(5)	206(1)	2668(1)	−231(1)	23(1)
C(6)	−5(1)	3827(1)	−1943(1)	28(1)
C(7)	−1628(2)	2969(1)	−2699(1)	43(1)
C(8)	−977(1)	1469(1)	1562(1)	23(1)
C(9)	−2097(1)	2330(1)	1563(1)	26(1)
C(10)	−3584(1)	202(1)	1474(1)	24(1)
C(11)	−1839(1)	224(1)	1498(1)	24(1)
C(12)	−4908(1)	−850(1)	1459(1)	29(1)
C(13)	−4368(2)	−2124(1)	1488(1)	41(1)
C(14)	2042(1)	2164(1)	2924(1)	24(1)
C(15)	3170(1)	1449(1)	3508(1)	29(1)
C(16)	3059(1)	3353(1)	4768(1)	27(1)
C(17)	1972(1)	3274(1)	3658(1)	26(1)
C(18)	3440(1)	4352(1)	5772(1)	31(1)
C(19)	2528(2)	5465(1)	5657(1)	38(1)
Cl(1)	2041(1)	8905(1)	5552(1)	39(1)
C(41)	540(3)	9984(3)	5594(2)	49(1)

[a] *U*(eq) is defined as one-third of the trace of the orthogonalized U_{ij} tensor.

TABLE 3: Reduced Atomic Coordinates ($\times 10^4$) and Equivalent Isotropic Displacement Parameters (Å^2 $\times$ 10^3) for the Monoclinic Form of 1,2-dichloroethane/TATM at −100 °C[a]

	x	*y*	*z*	*U*(eq)
S(1)	312(1)	−521(1)	8562(1)	56(1)
S(2)	1401(1)	4092(1)	11112(1)	62(1)
S(3)	4854(1)	2085(1)	8809(1)	68(1)
O(1)	−2086(2)	−770(2)	8303(2)	74(1)
O(2)	1551(2)	6395(2)	11089(2)	96(1)
O(3)	6582(2)	1263(2)	10640(2)	92(1)
C(1)	1664(2)	2374(2)	8726(2)	42(1)
C(2)	973(2)	1394(2)	8693(2)	41(1)
C(3)	1332(2)	387(2)	8684(2)	51(1)
C(4)	−646(2)	446(2)	8527(2)	46(1)
C(5)	−171(2)	1422(2)	8608(2)	45(1)
C(6)	−1794(2)	151(2)	8419(2)	54(1)
C(7)	−2594(2)	986(3)	8454(3)	87(1)
C(8)	1526(2)	3191(2)	9486(2)	41(1)
C(9)	1425(2)	2984(2)	10423(2)	52(1)
C(10)	1522(2)	4877(2)	10139(2)	51(1)
C(11)	1574(2)	4289(2)	9316(2)	46(1)
C(12)	1564(2)	6018(2)	10285(2)	68(1)
C(13)	1629(3)	6693(2)	9400(3)	94(1)
C(14)	2892(2)	2148(2)	8960(2)	44(1)
C(15)	3470(2)	2370(2)	8308(2)	57(1)
C(16)	4689(2)	1645(2)	9938(2)	49(1)
C(17)	3606(2)	1726(2)	9905(2)	47(1)
C(18)	5682(2)	1292(2)	10774(2)	60(1)
C(19)	5563(3)	993(3)	11772(3)	87(1)
Cl(1)	4640(2)	9172(10)	3657(8)	181(8)
C(41)	5539(12)	9753(11)	4878(11)	103(5)

[a] *U*(eq) is defined as one-third of the trace of the orthogonalized U_{ij} tensor.

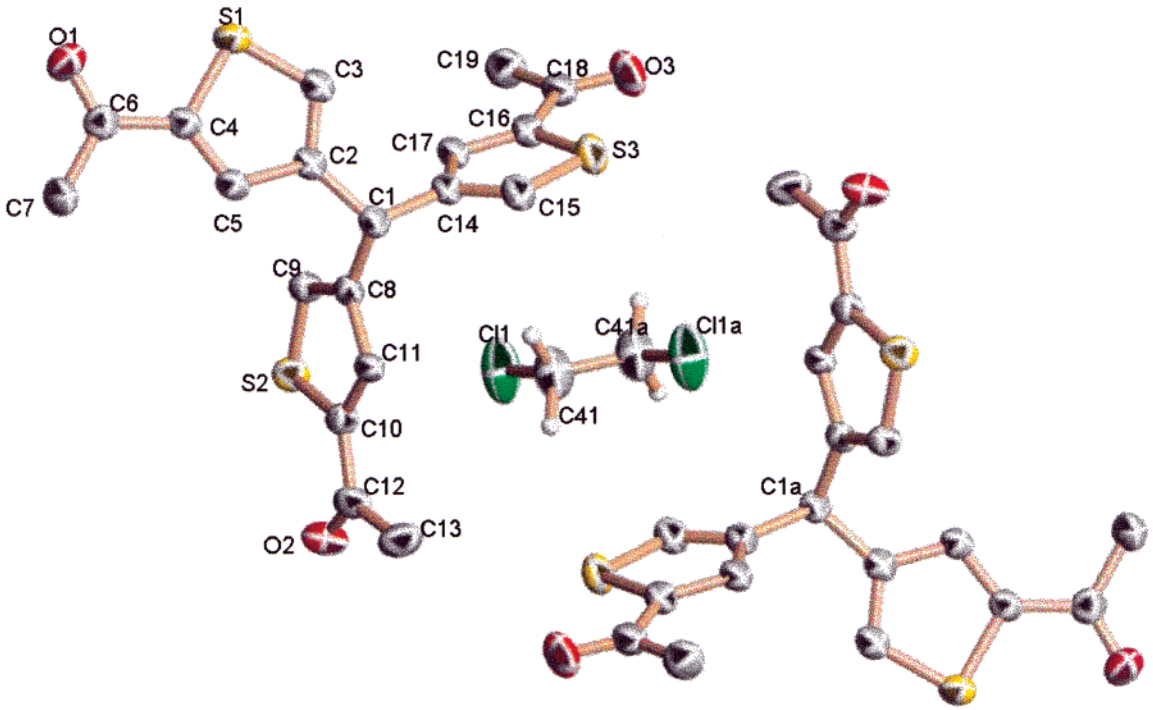

Figure 1. A schematic depiction of the unit cell of the triclinic form of 1,2-dichloroethane/TATM at −100 °C, showing the atomic numbering scheme for both forms.

value of 20 μs, and after left shifting to reach the echo maximum, the echo signals were Fourier transformed to obtain the NMR spectra. To improve the signal/noise ratio, spectra were symmetrized by adding the original spectrum to the same spectrum reflected about zero frequency. The temperature of the sample was lowered by passing cold nitrogen gas through the sample chamber, in conjunction with a heater in the gas stream, and the temperature was regulated by coupling the heater to a copper constantan thermocouple located close to the sample itself. The temperature of the sample was stable to within ±0.1 °C over the course of a measurement.

Quadrupolar echo spectra were simulated using the program MXQET.[33] This program takes into account variables such a 90° pulse length, pulse spacing τ_Q, and spectral line broadening. Simulated spectra were visually matched to experimental line shapes.

The deuterium T_1 data were determined using a home-built, phase-coherent pulsed NMR spectrometer operating a 44.7 MHz. The spectrometer was used with a 50 mm bore, 6.1 T (Bruker/Nalorac) superconducting magnet. The nuclear signal was digitized in a Nicolet Explorer digital oscilloscope, which was interfaced to an IBM personal computer. The computer was programmed to provide automatic temperature regulation for the sample and data acquisition. The temperature of the sample was electronically regulated to within ± 0.1 °C over the course of a measurement by a heater wound noninductively on a copper vessel surrounding the sample chamber, and a copper−constantan thermocouple attached to it. A second separate thermocouple located near the sample itself was used to record the actual sample temperature, which was accurate to within ± 0.5 °C.

The deuterium T_1 data were acquired using an inversion recovery pulse sequence modified for quadrupolar nuclei: $(\pi)_x-\tau-(\pi/2)_{\pm x}-\tau_Q-(\pi/2)_y-\tau_Q-$acquire. Typically, 12 values of τ were used to determine T_1 at each temperature. The pulse spacing, τ_Q, for the T_1 determination was 50 μs. The time between repetitions of the pulse sequence was always greater than $5T_1$. The amplitude of the signal for each τ value was determined from the integral over the echo peak. The echo integrals were fit using a nonlinear least-squares algorithm employing an exponential fitting function to obtain the relevant relaxation time parameters.

Results

(1) Single Crystal X-ray Diffraction. The crystals used for single crystal X-ray analysis were grown by slow evaporation. That is, a hot saturated solution of about 300 mg TATM in approximately 2 mL 1,2-dichloroethane was poured into a glass Petri dish, and the excess solvent was allowed to slowly evaporate over the course of 1−2 days. The first crystal chosen for analysis crystallized in the triclinic P-1 space group. The crystal data, data collection and final refinement data for the structure at −100 °C appear in Table 1. There are two host molecules in the unit cell, and they are related by a center of symmetry, giving one host TATM molecule in the asymmetric unit. There is one-half of a guest 1,2-dichloroethane molecule in the asymmetric unit, and the guest exists exclusively in the trans form. The center of inversion of the guest coincides with the center of inversion of the unit cell. The guest is disordered over three positions. A schematic illustration of the unit cell, showing the atomic numbering scheme, is depicted in Figure 1. Only one guest molecule is shown for clarity. The three guest site occupancy factors are 0.58, 0.23, and 0.19. A molecular packing diagram of the triclinic form, in the *ab* plane, (at −100 °C) appears in Figure 2. The TATM molecules form channels parallel to the crystallographic *c* axis in which the guest molecules reside. The term "channel" should be regarded with some reserve, however, as there is a significant constriction of the channel between adjoining guest molecules that prevents the guests' translation from one guest site to the next. In other words, there is a "bottleneck" in the channel between adjacent guests. Of the three acetylthienyl rings in the asymmetric unit, two participate in the formation of the guest channel, while the third interacts via $\pi-\pi$ stacking with the TATM host in the

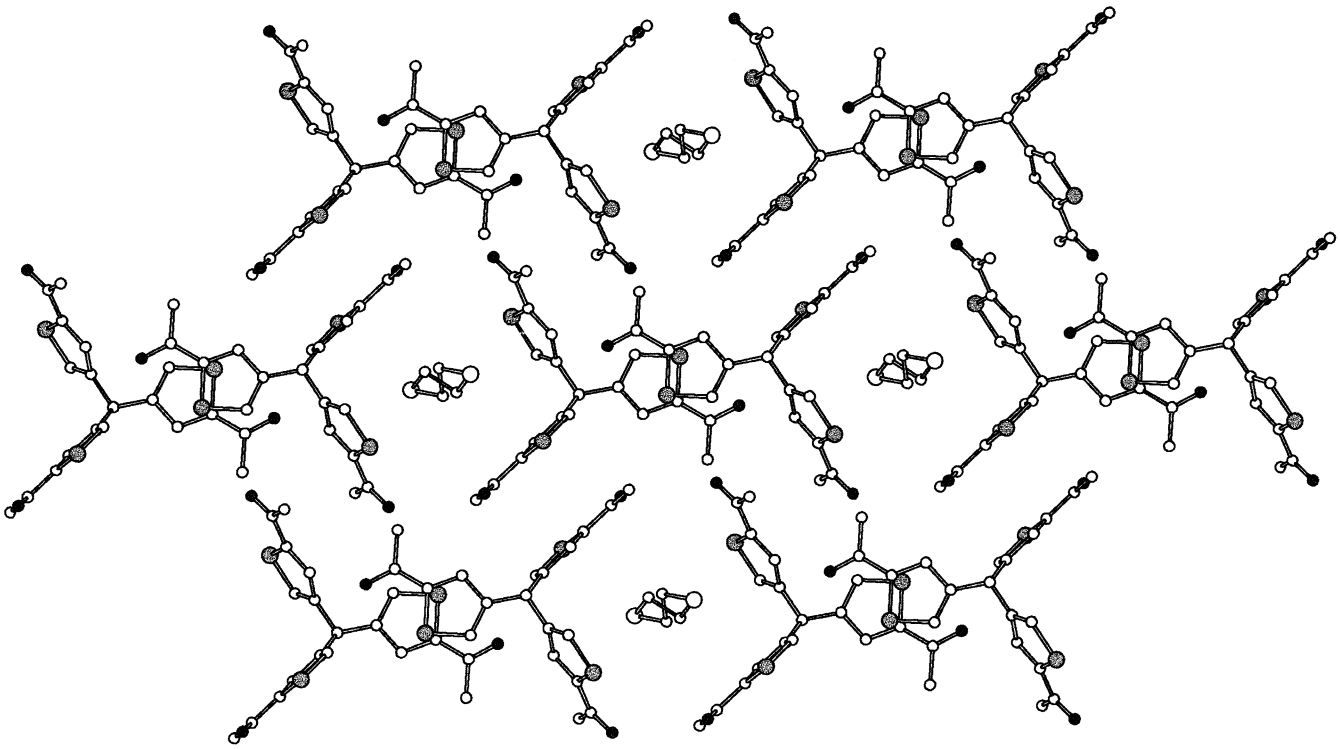

Figure 2. A packing diagram illustrating three ribbons in one sheet of the triclinic form of 1,2-dichloroethane/TATM at −100 °C.

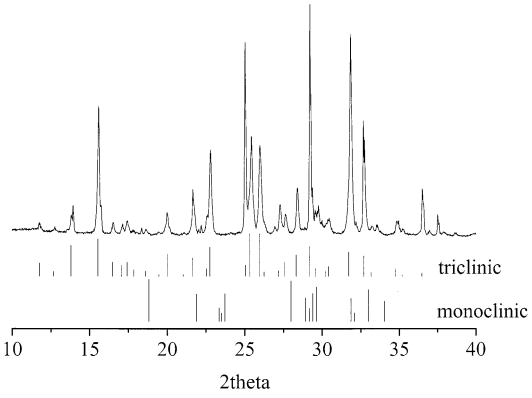

Figure 3. Powder X-ray diffractogram for 1,2-dichloroethane/TATM sample prepared by slow cooling (triclinic form only), along with peak positions calculated from the unit cell parameters of both forms. Note correlation with the triclinic form only.

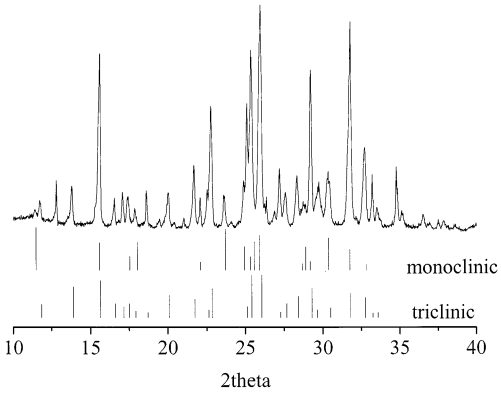

Figure 4. Powder X-ray diffractogram for 1,2-dichloroethane/TATM sample prepared by slow evaporation (triclinic and monoclinic mixture), along with peak positions calculated from the unit cell parameters of both forms. Note correlation with both triclinic and monoclinic form.

next unit cell to form an endless ribbon. In one layer, many ribbons are arranged parallel to one another to form sheets. Figure 2 depicts a short section of three such ribbons. Immediately on either side of a host cavity/guest molecule is located a pair of π stacked thienyl rings of adjacent ribbons, and on either side of the pair of π stacked thienyl rings is located a host cavity/guest molecule of adjacent ribbons.

We also found that the inclusion compound crystallizes in a monoclinic form, in the $P2_1/c$ space group. The difference between the two forms arises from the layering of ribbons in adjacent sheets (within one layer, the two forms are almost isostructural). In the triclinic form, the adjacent sheets are related by a unit cell translation, and the ribbons in adjacent sheets run parallel to one another. In the monoclinic form, the adjacent sheets are related by a *c* glide, and ribbons in adjacent sheets run in perpendicular directions. This suggests that the two forms are independently stable and do not interconvert on standing. Finally, we found that there is extensive weak aromatic C−H···O hydrogen bonding throughout the structure that apparently stabilizes the framework in both forms. Between layers there are only a few of these interactions, but within a layer there are many more. This suggests that stabilizing interactions within a layer are much stronger than the same interactions between layers. The crystal data for the monoclinic form at −100 °C appears in Table 1.

(2) Powder X-ray Diffraction. The powder X-ray diffraction pattern of the 1,2-dichloroethane/TATM sample obtained by slow cooling appears in Figure 3. The powder X-ray diffraction pattern of the same inclusion compound obtained by slow evaporation appears in Figure 4. The second pattern contains many more peaks than the first, so it may be reasonable to assume that the 1,2-dichloroethane/TATM inclusion compound obtained by slow cooling contains only one of the two phases, while the sample obtained by slow evaporation contains a mixture of both phases. In fact, a detailed analysis of the experimental powder X-ray diffraction peak positions (2θ) in comparison with those calculated from the respective single crystal structures show that the sample prepared by slow cooling

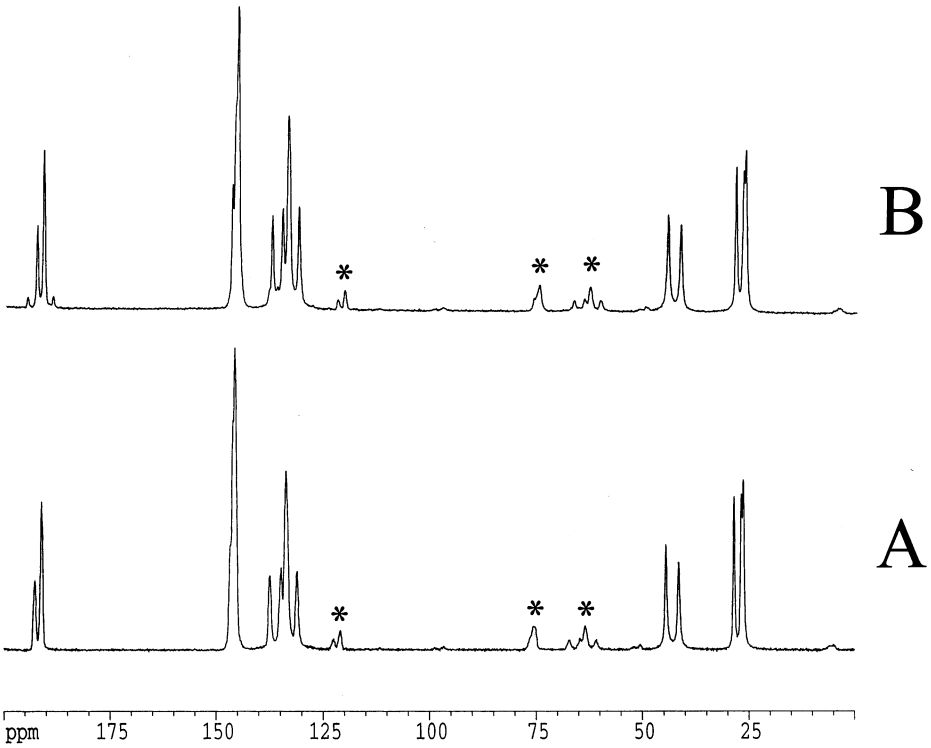

Figure 5. ^{13}C CP/MAS NMR spectra for 1,2-dichloroethane/TATM samples. Spinning sidebands are marked with an asterisk: (A) Sample prepared by slow cooling (triclinic form only). (B) Sample prepared by slow evaporation (triclinic and monoclinic mixture).

contains only the triclinic phase, while the sample prepared by slow evaporation contains both the triclinic and monoclinic phases. Figure 3 depicts the observed powder X-ray diffraction pattern for the inclusion compound prepared by slow cooling, along with the calculated reflection angles for the triclinic phase and the monoclinic phase. As can be seen in the Figure, there is very good correspondence between the observed reflection angles and the calculated reflection angles for the triclinic phase. In contrast, there is no agreement between the observed reflections and the calculated reflection angles for the monoclinic phase. This conclusively shows that the sample of 1,2-dichloroethane/TATM prepared by slow cooling contains only the triclinic phase.

The experimental powder X-ray diffraction pattern for the inclusion compound prepared by slow evaporation appears in Figure 4, along with the calculated angles for the triclinic phase and the monoclinic phase. In this case, there are a number of reflections that cannot be accounted for by the calculated angles for the triclinic cell. However, these reflections can be assigned to calculated reflections for the monoclinic cell. Therefore, this shows that the sample of 1,2-dichloroethane/TATM prepared by slow evaporation contains a mixture of the triclinic phase and the monoclinic phase.

(3) ^{13}C CP/MAS NMR. The ^{13}C CP/MAS NMR spectrum of 1,2-dichloroethane/TATM prepared by slow cooling appears in Figure 5A. As was noted in the previous section, this sample contains only the triclinic phase. The multiplicity of the TATM carbonyl signal at about 192 ppm is three, and the multiplicity of the TATM methyl signal at about 28 ppm is also three. This implies that there is one TATM molecule in the asymmetric unit for this sample, as there are three carbonyl groups and three methyl groups in one TATM molecule. This result agrees with the single-crystal X-ray diffraction analysis. In the single-crystal structure, there are two TATM molecules in the unit cell, and a center of symmetry relates these two host molecules. The multiplicity of the TATM thienyl ring quaternary carbons at 146 ppm (they remain on dipolar dephasing) is six, as is the multiplicity of the TATM thienyl ring tertiary C−H carbons at about 135 ppm. As there are six quaternary carbons and six tertiary carbons in one TATM molecule, this provides further support. The 1,2-dichloroethane signal resonates at 44.5 ppm (the signal at 42 ppm comes from the TATM methine carbon), which is 0.6 ppm downfield of the resonance position of 1,2-dichloroethane in the neat liquid (43.9 ppm). This implies that 1,2-dichloroethane's nuclei are deshielded in the TATM inclusion compound relative to its state in the pure liquid.

The ^{13}C CP/MAS NMR spectrum of the 1,2-dichloroethane/TATM inclusion compound prepared by slow evaporation appears in Figure 5B. As was noted in the last section, this sample contains a mixture of triclinic and monoclinic phases. The spectrum appears identical to the spectrum of the sample prepared by slow cooling. However, now there is one small peak to high field of the TATM carbonyl signals and one small peak to low field of the TATM carbonyl signals. These peaks are not spinning sidebands, as identical spinning rates were used in the acquisition of the two spectra. Therefore these small peaks must be from the small amount of monoclinic 1,2-dichloroethane/TATM in the sample prepared by slow evaporation. There is also a small peak visible at 136 ppm partially hidden under the main signal from the TATM tertiary thienyl signal. There are likely also other weak signals corresponding to the other host TATM carbons and 1,2-dichloroethane guest, but they may be hidden underneath the larger signals corresponding to the triclinic 1,2-dichloroethane form. Thus we see agreement between results obtained from powder X-ray diffraction and those obtained from ^{13}C CP/MAS NMR, demonstrating the complementary information available from these two experimental techniques.

(4) Deuterium NMR. Initially, the NMR dynamic spectra were treated as an independent data set. That means that a likely model was chosen, in this case consistent with rotational isomerism as in the gas phase, and analyzed to be internally

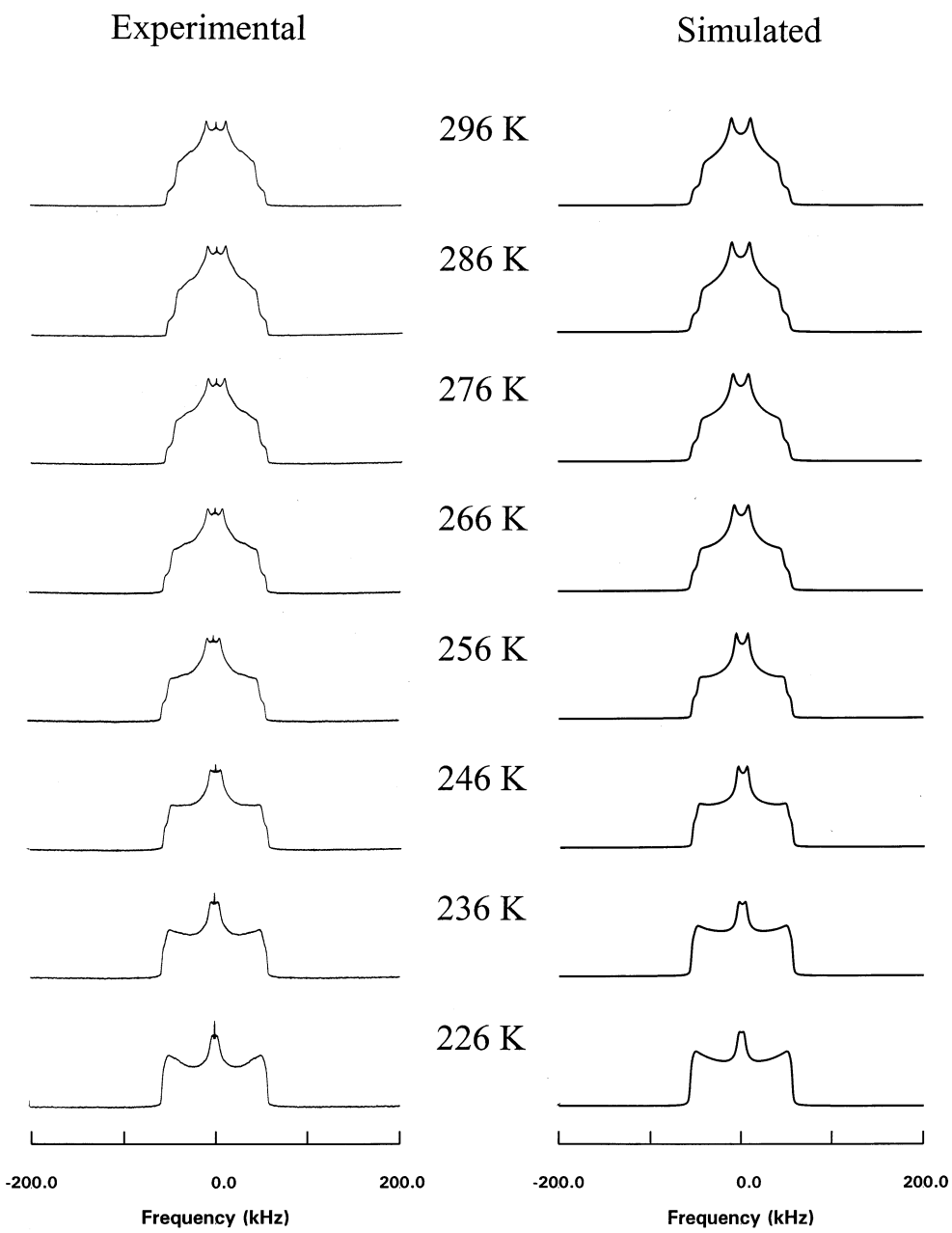

Figure 6. Experimental (left) and simulated (right) solid-state deuterium NMR spectra for the 1,2-dichloroethane-d_4/TATM inclusion compound at the temperatures indicated, based on Model 1 (trans−gauche conformational equilibrium). Dynamic and conformational data extracted by simulating the experimental spectra appear in Table 4.

consistent. This was then placed alongside the model from single-crystal XRD to check for consistency among techniques. The initial NMR model then had to be abandoned, as it was not possible to arrive at a consistent model. A second dynamic model was then chosen to conform to the structural data. Both NMR models are presented, as there is an important lesson to be learned regarding uniqueness of models and the importance of complementary approaches.

(a) Model 1: Trans−Gauche Conformational Equilibrium. The deuterium NMR spectra (from 296 to 226 K) for the 1,2-dichloroethane-d_4/TATM inclusion compound, along with simulated spectra, appear in Figure 6. The details of the parameters used in these simulations are outlined below. It should be noted that the sample prepared for analysis by deuterium NMR spectroscopy was made by slow cooling of a hot saturated solution, and therefore contains only the triclinic phase. The spectra were simulated by considering the possibility of conformers for the guest, as in the gas phase, when one CD_2Cl group is held fixed, while the other is rotated 360° about the C−C bond. The lowest energy trans conformer has a 180° dihedral angle between the two C−Cl bonds. The two higher energy gauche conformers have dihedral angles of 60° and −60° between the two C−Cl bonds. This gives three potential energy minima. There are also three potential energy maxima. The highest energy maximum corresponds to a dihedral angle of 0° between the two C−Cl bonds, denoted as the *eclipsed* (0°) transition state. The two lower energy maxima correspond to a 120° dihedral angle between the C−Cl bonds, denoted the *eclipsed* (120°) transition state. A potential energy diagram based on this scheme is depicted in Figure 7, which shows the rotational potential energy of the guest as a function of the dihedral angle between the two C−Cl bonds, and Newman projections of the 1,2-dichloroethane-d_4 conformers an each potential energy minimum and maximum.

In this model, the guest 1,2-dichloroethane molecule interconverts between the trans and gauche potential energy minima

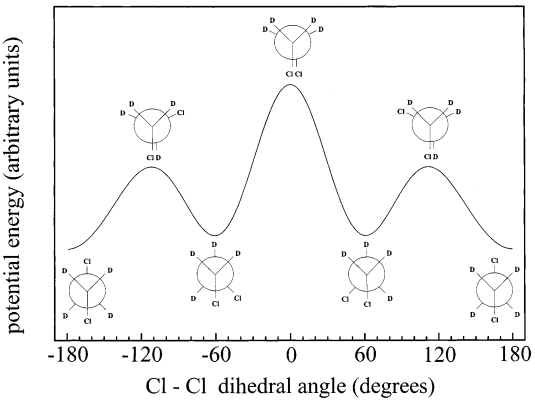

Figure 7. A schematic potential energy diagram illustrating the conformers present (as Newman projections) at the three potential energy minima and the three potential energy maxima as the 1,2-dichloroethane is rotated 360° about the carbon−carbon bond, based on Model 1.

TABLE 4: A Table of Guest Conformational/Dynamic Parameters Obtained by Simulating (Model 1) the Solid-State Deuterium NMR Spectra of 1,2-dichloroethane-d_4 in TATM at the Temperatures Indicated

T (K)	$k_{t\rightarrow g}$[a]	$k_{g\rightarrow t}$[b]	$k_{g\rightarrow g}$[c]	P_{trans}[d]	$P_{gauche1}$[e]	$P_{gauche2}$[f]
296	7.74×10^7	1.45×10^8	0	0.484	0.258	0.258
286	5.04×10^7	9.92×10^7	0	0.496	0.252	0.252
276	2.45×10^7	5.10×10^7	0	0.510	0.245	0.245
266	1.44×10^7	3.12×10^7	0	0.520	0.240	0.240
256	9.20×10^6	2.16×10^7	0	0.540	0.230	0.230
246	4.40×10^6	1.12×10^7	0	0.560	0.220	0.220
236	1.89×10^6	5.22×10^6	0	0.580	0.210	0.210
226	1.20×10^6	3.60×10^6	0	0.600	0.200	0.200

[a] The rate of conversion from the trans conformer to the gauche conformers, in jumps per second. [b] The rate of conversion from the gauche conformers to the trans conformer, in jumps per second. [c] The rate of conversion of one gauche conformer to the other gauche conformer, in jumps per second. The ^{2}H NMR spectra were simulated at all temperatures by approximating a rate of zero. [d] The fractional population of the trans conformer at each temperature. [e] The fractional population of one of the two gauche conformers at each temperature. [f] The fractional population of the other gauche conformer at each temperature.

by performing 120° jumps about the C−C bond. According to the simulated deuterium NMR spectra, the trans conformer has a higher fractional population (and lower potential energy), while the two gauche conformers have lower, and equal, fractional populations (and higher potential energy). As the temperature is lowered below room temperature, the fractional population of the lower energy trans conformer increases at the expense of the fractional populations of the two higher energy gauche conformers. This temperature−population behavior is also observed in the pure liquid state and pure gaseous state of 1,2-dichloroethane, for which trans−gauche isomerism is known to exist.[5] According to the simulated ^{2}H NMR spectra for 1,2-dichloroethane-d_4/TATM, at room temperature (296 K) the population of the trans conformer is 48.4%, while the populations of the two gauche conformers are both 25.8% each. At the lowest temperature measured, 226 K, the population of the trans conformer increases to approximately 60%, while the same for the two gauche conformers decreases to about 20% each. At each temperature measured, the fractional populations appear in Table 4. If one calculates the equilibrium constant (K_{eq}) at each temperature as the ratio of the two populations (see Table 4), it is possible to determine the enthalpy difference between the two conformers from the slope of a plot of $\ln K_{eq}$ against inverse temperature. This graph appears in Figure 8, and we

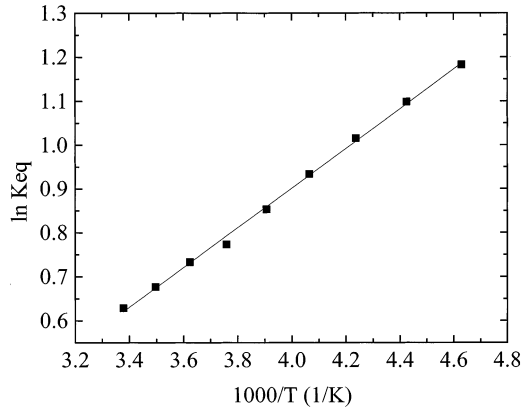

Figure 8. A plot of the natural logarithm of the equilibrium constant against inverse temperature for the conformational equilibrium of 1,2-dichloroethane-d_4 in TATM, based on Model 1. The equilibrium constant was defined at each temperature as the fractional population of the trans conformer divided by the fractional population of the gauche conformer. From the slope of a best fit curve, an energy difference between the trans and gauche conformers of 3.75 (±0.06) kJ/mol was determined, the trans conformer being lower in energy.

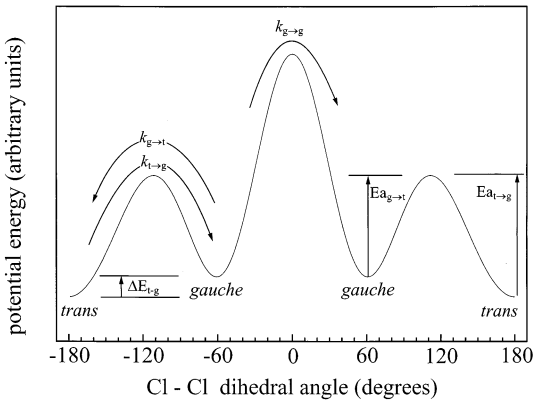

Figure 9. A schematic potential energy diagram depicting the three independent rates, two of the three independent activation barriers and the energy difference between the potential energy minima with regards to the conformational equilibrium for 1,2-dichloroethane in TATM, based on Model 1. The conformers present at the three potential energy minima and the three potential energy maxima are the same as those in Figure 7.

calculate the enthalpy difference between the trans and gauche conformers as 3.75 (±0.06) kJ mol^{-1}.

When considering the rate of interconversion between the trans and gauche conformers, calculated from the deuterium NMR spectra, there are actually three different rates to consider, as depicted in the potential energy diagram of Figure 9. We can assign $k_{g\rightarrow t}$ as the rate of conversion of the gauche conformers to the trans conformer. Conversely, $k_{t\rightarrow g}$ is the rate of conversion of the trans conformer to the gauche conformers. Finally, $k_{g\rightarrow g}$ is the rate of conversion of one gauche conformer to the other gauche conformer. As the trans conformer has the lowest energy in this case, $k_{g\rightarrow t}$ has the smallest activation barrier, and hence the fastest rate, of the three at any particular temperature. The rate of conversion $k_{t\rightarrow g}$ has a higher activation energy and hence a smaller rate than $k_{g\rightarrow t}$. When the 1,2-dichloroethane molecule interconverts from one gauche conformer to the other gauche conformer, it must go through the highest energy maximum, the *eclipsed* (0°) transition state. Thus $k_{g\rightarrow g}$ has the highest activation energy and the smallest rate. The three rates at each measured temperature that we used in the simulations appear in Table 4. Note that we approximated a rate of 0 Hz at all temperatures for $k_{g\rightarrow g}$. We considered this

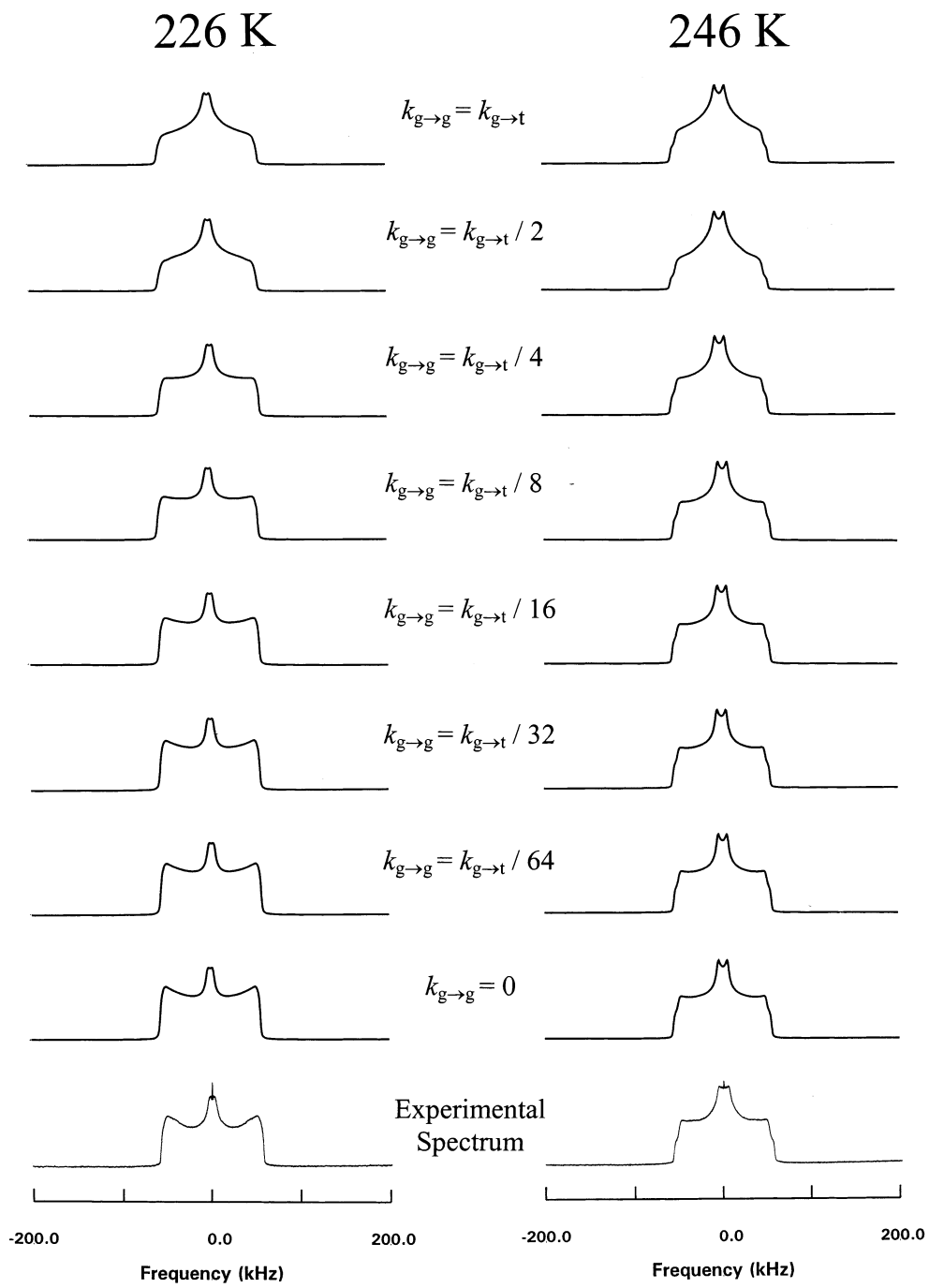

Figure 10. Experimental and simulated (Model 1) solid-state deuterium NMR spectra for the 1,2-dichloroethane-d_4/TATM inclusion compound at 226 and 246 K. The experimental spectrum at each temperature appears at the bottom. Eight simulated spectra were performed at each temperature, the difference between them being the rate of conversion about the gauche-gauche barrier. The rate $k_{g\to g}$ is varied as a function of the rate $k_{g\to t}$, as depicted in the figure.

situation in detail for the deuterium NMR spectrum at two temperatures (226 and 246 K). We performed simulations using fixed $k_{g\to t}$ and $k_{t\to g}$ rates of interconversion. We varied $k_{g\to g}$ as a function of $k_{g\to t}$. The simulations appear in Figure 10. By comparing the experimental ^{2}H NMR spectra at 226 and 246 K with the simulated spectra, it can be concluded that the rate $k_{g\to g}$ is at most 1/64 times as large as $k_{g\to t}$. That is, $k_{g\to g}$ is somewhere between this value and zero. However, from the simulated spectra, we are unable to determine the rate $k_{g\to g}$ precisely at each temperature, so we simply used a rate of 0 Hz, this is only an approximation. The spectra are invariant to the rate of $k_{g\to g}$ when it is any value less than 1/64 times as large as $k_{g\to t}$. On the other hand, we were able to determine $k_{g\to t}$ and $k_{t\to g}$ precisely at each temperature, these rates appear in Table 4. By plotting ln $k_{g\to t}$ and ln $k_{t\to g}$ against inverse temperature (see Figure 11), we calculate that the activation barrier to go from the trans conformer to the gauche conformers ($E_{a_{t\to g}}$) is 33.0 (±0.9)kJ mol^{-1}, while the activation barrier to go from the gauche conformers to the trans conformer ($E_{a_{g\to t}}$) is 29.2 (±0.9) kJ mol^{-1}. In theory, the energy difference ΔH_{gt} between the trans and gauche conformers added to $E_{a_{g\to t}}$ should equal $E_{a_{t\to g}}$. The former sum is 3.75 kJ mol^{-1} + 29.2 kJ mol^{-1} = 32.9 kJ mol^{-1}, the latter is 33.0 kJ mol^{-1}, showing good agreement. From the spectra, we cannot quantitatively determine the magnitude of the gauche → gauche barrier, we can only say it is much greater than the other two activation energies.

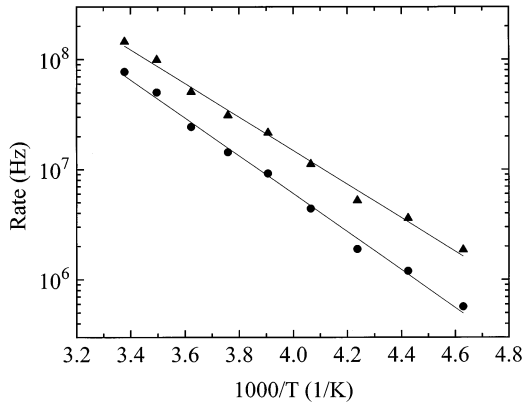

Figure 11. A plot of reorientational rate against inverse temperature on a semilogarithmic scale, for the conformational equilibrium of 1,2-dichloroethane-d_4 in TATM, according to Model 1. The rate $k_{g\rightarrow t}$ appears as triangles and the rate $k_{t\rightarrow g}$ appears as circles. From the slope of best fit curves, activation barriers $E_{a_{g\rightarrow t}} = 29.2$ ($\pm$0.9) kJ/mol and $E_{a_{t\rightarrow g}} = 33.0$ ($\pm$0.9) kJ/mol were determined.

The literature on activation barriers for internal rotation about the C−C bond in 1,2-dichloroethane is sparse indeed. From gas phase heat capacity measurements, Gwinn and Pitzer determined a barrier of 11.30 kJ mol^{-1} between the trans and gauche conformers:[37] they did not specify whether the barrier referred to $E_{a_{g\rightarrow t}}$ or $E_{a_{t\rightarrow g}}$. From a force model calculation, Bernstein found that the trans-gauche barrier is 11.76 kJ mol^{-1} and the gauche-gauche barrier is a much larger 18.80 kJ mol^{-1}.[38] For our motional model, the barriers $E_{a_{g\rightarrow t}}$ and $E_{a_{t\rightarrow g}}$ for 1,2-dichloroethane in TATM are both much larger than not only the two trans−gauche barriers listed, but also the gauche−gauche barrier.

(b) Model 2: NMR Model Based on Motion between Disordered Positions as Shown in the X-ray Structure (Restricted Cl Motion). Unfortunately, the single-crystal structure of the triclinic form shows no evidence for the existence of a gauche conformer, or for that matter, rotation about the C−C bond of the 1,2-dichloroethane guest. Although the fit between the simulated and experimental ^{2}H NMR spectra using Model 1 are excellent, one must be aware that the dynamic models used in spectral simulations are not unique. More than one set of simulations based on particular motional models may fit the experimental spectra. Still, this model does not agree with the disorder of the guest as elucidated from our crystal structure, so we attempted to simulate the ^{2}H NMR spectra based on the disorder inherent in the crystal structure. The sample used for deuterium NMR analysis was prepared by slow cooling, so it contains only the triclinic form. We performed crystal structure analyses for the triclinic form at 298 and 173 K. At both of these temperatures, the guest is disordered over three sites. We considered all possible exchanges between guest sites that do not involve an end-to-end exchange of the terminal Cl atoms. We determined the Euler angles relating the deuterons exchanging over three sites and entered the angles into the MXQET simulation program. Unfortunately, we were unable to obtain a satisfactory fit between the experimental and simulated ^{2}H powder spectra. Finally, as part of these simulations, we were able to show that the deuterium NMR spectra are relatively insensitive to 180° flips about the Cl−Cl axis, and although this motion may be present it does not explain the observed results.

(c) Model 3: Two-Fold Flip (Large Scale Cl Motion). The failure of Model 2 led us to consider a model that includes end-to-end exchange of the terminal Cl atoms. The simplest such motion is a 2-fold reorientation about an axis through the center of mass of the guest and perpendicular to the Cl−C−C−Cl plane of the trans conformer. The guest performs 180° jumps about this axis to rotate back into itself (see Figure 12). Therefore, this motion would be invisible in the single-crystal diffraction experiment. We were able to obtain a satisfactory fit with the experimental spectra over the range 296 K to 186 K, as depicted in Figure 13. The rate of the 2-fold reorientation goes from 5×10^7 Hz at 296 K to 3×10^4 Hz at 186 K. A plot of rate vs inverse temperature appears in Figure 14. From the slope of the best-fit line, we calculate an activation barrier of 30.1 ($\pm$0.6) kJ mol^{-1}.

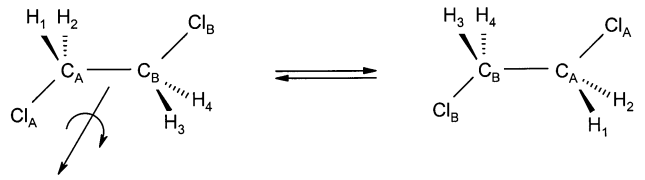

Figure 12. A schematic depiction of the reorientation of the 1,2-dichloroethane guest in TATM, according to Model 3 (2-fold flip).

It should be noted that although the trans−gauche conformational model (Model 1) was able to fit the experimental spectra very well in the region 296−226 K, it was unable to match the experimental spectra in the region 216−186 K. This provides further support for the correctness of the 2-fold flip model (Model 3).

Another feature of this model is that the 1,2-dichloroethane molecule performs small angle librations about the 2-fold axis within the two potential wells of the C_2 flip. That is, this motion ($k \gg 10^8$ Hz) is superimposed on the 2-fold flip. The amplitude of this motion increases with temperature, going from $\pm$3° at 226 K to $\pm$28° at 296 K. The modeled librational angle at each temperature is plotted in Figure 15.

The profile of ^{2}H spin−lattice relaxation for 1,2-dichloroethane-d_4/TATM, as a function of inverse temperature, is presented in Figure 16. Changes in T_1 in this temperature range result from changes in the rate of the above-mentioned 2-fold flips. It is apparent from the T_1 profile that the correlation time of the motion is exclusively on the slow motion side of the T_1 minimum (i.e., the rate of motion k is less than the Larmor precession frequency). The ^{2}H spin−lattice relaxation time at ambient temperature, the highest temperature measured, is 56.1 ms. The relaxation time at 232.8 K, the lowest temperature measured, increases to 202 ms. (We were somewhat hesitant to acquire T_1 data at temperatures above room temperature, as from our experience, TATM inclusion compounds generally decompose at these temperatures.) From the slope of the curve in the linear region (at intermediate temperatures) we calculate that the activation energy for the 2-fold flip is 25.4 ($\pm$ 0.3) kJ mol^{-1}. This compares with an activation energy of 30.1 ($\pm$ 0.6) kJ mol^{-1} determined from ^{2}H NMR spectral simulations quoted above. Note that the lack of a complete T_1 minimum precluded a detailed fit of the T_1 data, from which one can determine the correlation time (τ_c) of the motion as a function of temperature ($\tau_c \propto k^{-1}$). However the similarity of the activation energies from ^{2}H spectra and ^{2}H T_1 data lends support to the accuracy of the 2-fold flip model.

Conclusions

The combined ^{2}H NMR and single-crystal structural data suggest that the barrier to internal rotation of the 1,2-dichloroethane molecule is very high in the TATM cavity, as it is in the pure guest solid phase. One way that this may happen is if the cavity shape and the trans form of the molecule show some

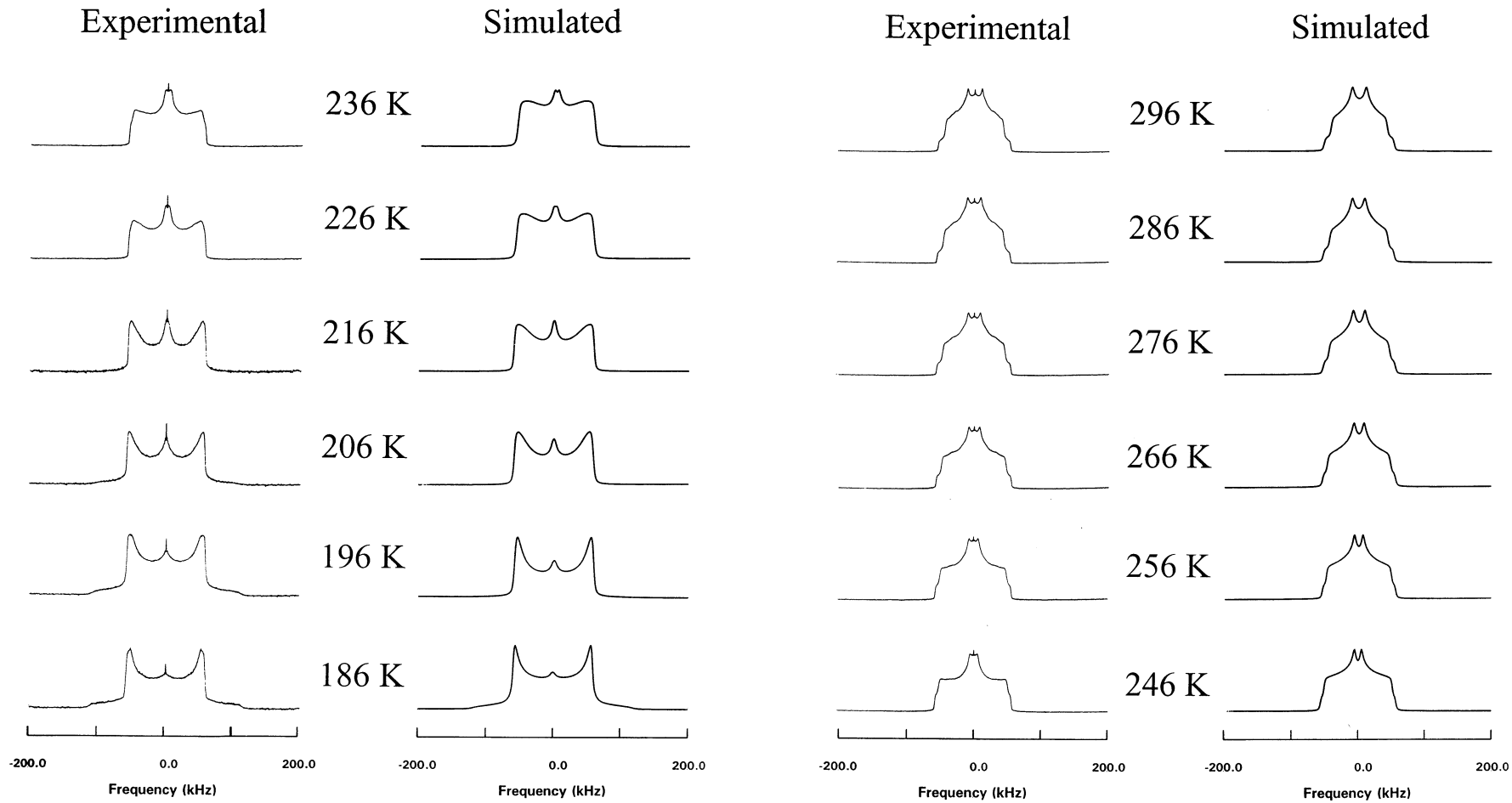

Figure 13. Experimental and simulated solid-state deuterium NMR spectra for the 1,2-dichloroethane-d_4/TATM inclusion compound, based on Model 3 (2-fold flip).

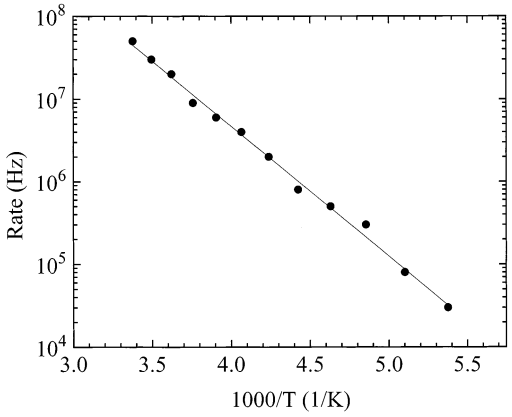

Figure 14. A plot of the rate of 2-fold reorientation against inverse temperature for the 1,2-dichloroethane-d_4 guest (according to Model 3). The rate at each temperature was determined by simulating the experimental ^{2}H NMR spectra. A best fit line indicates an activation barrier of 30.1 ($\pm$ 0.6) kJ mol^{-1}.

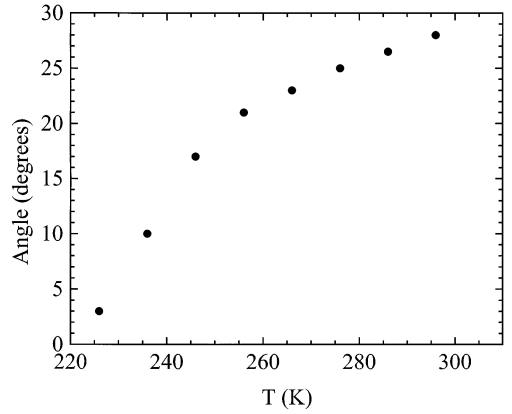

Figure 15. A plot of angle of libration within the two potential energy wells against temperature for the 1,2-dichloroethane-d_4 guest, based on Model 3. The angle at each temperature was determined by simulating the experimental ^{2}H NMR spectra.

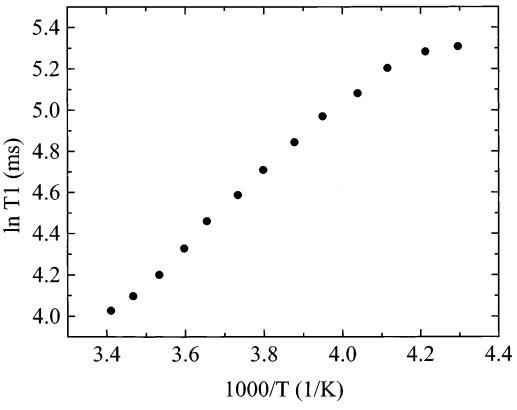

Figure 16. A plot of the deuterium spin−lattice relaxation time of the 1,2-dichloroethane-d_4 guest as a function of inverse temperature. From the slope of the curve in the linear region, an activation energy of 25.4 ($\pm$0.3) kJ/mol for the 2-fold flip (Model 3) was determined.

complementarity in terms of guest−host interactions. The Cl atoms are likely to play a key role in locating the molecule in the cavity, although this must be determined during guest−host assembly of the crystal. We note that the TATM host is one of the most versatile in adopting a variety of structures with different guests.

One crucial point to be taken from this work is that although a simple dynamic model may produce calculated simulations that fit the ^{2}H NMR experimental spectra very accurately, one must realize that these models are not unique, and that information gained from other experimental techniques (such as single-crystal X-ray diffraction) can often provide information that will support or refute a proposed model, as was the case here for 1,2-dichloroethane/TATM. In coming up with a proposed dynamic model, one must make sure that it is consistent with information obtained from all of the other relevant experiments performed.

Acknowledgment. We are grateful to the Natural Sciences and Engineering Research Council of Canada (NSERC) for financial support of part of this work, in the form of a post-graduate scholarship to P. S. and operating grants to G. P. and J. R.

Supporting Information Available: Bond lengths, bond angles, anisotropic displacement parameters. and hydrogen reduced atomic coordinates for both the triclinic and monoclinic forms have been deposited as Supporting Information. In addition, we have included two tables of experimental and calculated angles of reflections (powder XRD), along with their relative intensities, for the pure triclinic sample and the triclinic/monoclinic mixture. This material is available free of charge via the Internet at http://pubs.acs.org.

References and Notes

(1) Milberg, M. E.; Lipscomb, W. N. *Acta Crystallogr.* **1951**, *4*, 369.
(2) Gutowsky, H. S.; Pake, G. E. *J. Chem. Phys.* **1950**, *18*, 162.
(3) Mizushima, S.; Shimanouchi, T.; Harada, I.; Abe, Y.; Takeuchi, H. *Can. J. Phys.* **1975**, *53*, 2085.
(4) Ragle, J. L. *J. Phys. Chem.* **1959**, *63*, 1395.
(5) Mizushima, S. *Structure of Molecules*; Academic Press: New York, 1954.
(6) Garg, S. K.; Davidson, D. W.; Gough, S. R.; Ripmeester, J. A. *Can. J. Chem.* **1979**, *57*, 635.
(7) Hartley, H.; Thomas, N. G. *J. Chem. Soc.* **1906**, *89*, 1013.
(8) Bin Din, L.; Meth-Cohn, O. *J. Chem. Soc., Chem. Commun.* **1977**, *21*, 741.
(9) Yakubov, A. P.; Sudarushkin, Y. K.; Belen'kii, L. I.; Gol'dfarb, Y. L. *J. Org. Chem. (USSR)* **1973**, *9*, 1549.
(10) Marsh, R. E. *Acta Crystallogr.* **1994**, *B50*, 112.
(11) Van Rooyen, P. H.; Roos, H. M. *Acta Crystallogr.* **1991**, *C47*, 2468.
(12) Dillen, J. L. M.; Roos, H. M. *Acta Crystallogr.* **1992**, *C48*, 2229.
(13) Roos, H. M.; Dillen, J. L. M. *Acta Crystallogr.* **1992**, *C48*, 1882.
(14) Van Rooyen, P. H.; Roos, H. M. *Acta Crystallogr.* **1991**, *C47*, 2718.
(15) Pang, L.; Hynes, R. C.; Whitehead, M. A. *Acta Crystallogr.* **1994**, *C50*, 615.
(16) Pang, L.; Brisse, F. *Acta Crystallogr.* **1994**, *C50*, 1947.
(17) Pang, L.; Brisse, F. *Can. J. Chem.* **1994**, *72*, 2318.
(18) Dauter, Z.; Wilson, K. S. Diffraction Techniques. In *Comprehensive Supramolecular Chemistry*; Atwood, J. L., Davies, J. E. D., MacNicol, D. D., Vogtle, F., Eds. Elsevier Science, Ltd.: New York, 1996; Vol. 8, pp 1−31.
(19) Fyfe, C. A. *Solid State NMR for Chemists*; C. F. C. Press: Guelph, Ontario, Canada, 1983.
(20) Spiess, H. W. *Adv. Polym. Sci.* **1985**, *66*, 23.
(21) Davis, J. H. In *Isotopes in the Physical and the Biomedical Sciences*; Buncel, E., Jones, J. R., Eds. Elsevier Science: Amsterdam, 1991.
(22) Griffin, R. G. *Methods. Enzymol.* **1981**, *72*, 108.
(23) Brauniger, T.; Poupko, R.; Zimmerman, H.; Luz, Z. *J. Chem. Soc., Perkin Trans. 2* **1997**, 1255.
(24) Ratcliffe, C. I. *J. Phys. Chem.* **1994**, *98*, 8, 10935.
(25) Penner, G. H.; Chang, Y. C. P.; Hutzal, J. *Inorg. Chem.* **1999**, *38*, 2868.
(26) Sidhu, P. S.; Penner, G. H.; Jeffrey, K. R.; Zhao, B.; Wang, Z. L.; Goh, I. *J. Phys. Chem.* **1997**, *101*, 1B, 9087.
(27) Sidhu, P. S.; Bell, J.; Penner, G. H.; Jeffrey, K. R. *Can. J. Chem.* **1996**, *74*, 1784.
(28) Schmider, J.; Muller, K. *J. Phys. Chem.* **1998**, *102*, 2A, 1181.
(29) Duer, M. J.; He, H.; Kolodziejski, W.; Klinowski, J. *J. Phys. Chem.* **1994**, *98*, 1198.
(30) Shantz, D. F.; Lobo, R. F. *J. Phys. Chem.* **1998**, *102*, 2B, 2339.
(31) Sato, T.; Kunimori, K.; Hayashi, S. *Phys. Chem. Chem. Phys.* **1999**, *1*, 3839.

(32) Davis, J. H.; Jeffrey, K. R.; Bloom, M.; Valic, M. I.; Higgs, T. P. *Chem. Phys. Lett.* **1976**, *42*, 390.
(33) Greenfield, M. S.; Ronemus, A. D.; Vold, R. L.; Vold, R. R.; Ellis, P. D.; Raidy, T. R. *J. Magn. Reson.* **1987**, *72*, 89.
(34) Thomas, A. F. *Deuterium Labeling in Organic Chemistry*; Meredith Corp.: New York, 1971.
(35) Sidhu, P. S.; Ripmeester, J. A. *J. Supramol. Chem.* **2001**, *1*, 63.
(36) Gabe, E. J.; LePage, Y.; Charland, J. P.; Lee, F. L.; White, P. S *J. Appl. Crystallogr.* **1989**, *22*, 384.
(37) Gwinn, W. G.; Pitzer, K. S. *J. Chem. Phys.* **1948**, *16*, 303.
(38) Bernstein, H. J. *J. Chem. Phys.* **1949**, *17(3)*, 258.